

A Read Margin Enhancement Circuit with Dynamic Bias Optimization for MRAM

Renhe Chen, Albert Lee, Yongqi Hu, and Xufeng Kou, *Senior Member, IEEE*

Abstract—This brief introduces a read bias circuit to improve readout yield of magnetic random access memories (MRAMs). A dynamic bias optimization (DBO) circuit is proposed to enable the real-time tracking of the optimal read voltage across process-voltage-temperature (PVT) variations within an MRAM array. It optimizes read performance by adjusting the read bias voltage dynamically for maximum sensing margin. Simulation results on a 28-nm 1Mb MRAM macro show that the tracking accuracy of the proposed DBO circuit remains above 90% even when the optimal sensing voltage varies up to 50%. Such dynamic tracking strategy further results in up to two orders of magnitude reduction in the bit error rate with respect to different variations, highlighting its effectiveness in enhancing MRAM performance and reliability.

Index Terms—Magnetic random access memory, read margin enhancement, tunneling magnetoresistance ratio, readout mechanism, bias voltage optimization

I. INTRODUCTION

MAGNETIC random access memory (MRAM) has emerged as a compelling candidate for the next generation non-volatile memory, which offers fast operating speed (<10 ns), low energy consumption (<1 pJ/bit), and long endurance ($>10^9$) [1], [2]. So far, different programming mechanisms, such as spin-transfer torque (STT), spin-orbit torque (SOT), and voltage-controlled magnetic anisotropy (VCMA) effects have been proposed to enhance the energy efficiency of data storage [3]–[5]. On the other hand, the read operation of MRAM relies on the tunneling magnetoresistance effect, where the resistance of a magnetic tunnel junction (MTJ) depends on the relative magnetic orientations between the fixed layer and the free layer, as shown in Fig.1(a). In this context, the data stored in an MRAM cell can be read by comparing the resistance of bit-cell against a reference via a sense amplifier (SA) (Fig. 1(b)).

A major challenge for MRAM read operation is the small tunneling magnetoresistance ratio (TMR) which characterizes the resistance difference between the parallel (P) and anti-parallel (AP) states. This, along with process-voltage-temperature (PVT) variations, results in narrow sensing margins which are inevitably vulnerable to thermal noise and circuit mismatch-induced offset, therefore causing read errors.

This work is sponsored partly by the National Key R&D Program of China(Grant No.2021YFA0715503), National Natural Science Foundation of China(GrantNo.92164104), and Xufeng Kou acknowledges the support from the Shanghai Rising-Star program(Grant No.21QA1406000).

Renhe Chen, Zirui Wang, and Xufeng Kou are with the School of Information Science and Technology, ShanghaiTech University, Shanghai 201210, China (e-mail: kouxf@shanghaitech.edu.cn).

Albert Lee and Di Wu are with the Inston Tech, Suzhou 215121, China (e-mail: albertlee@instontech.com, diwu@instontech.com).

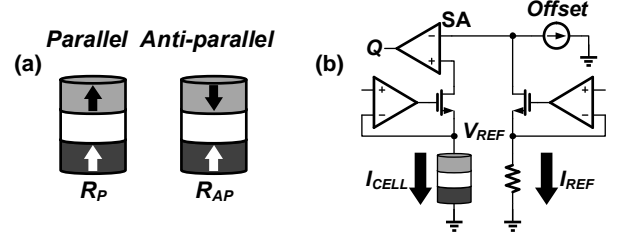


Fig. 1. (a) Parallel and anti-parallel states of MTJ. (b) Schematic of current based sensing in MRAM.

To address such an issue, calibration modules or offset compensation circuits have been introduced into MRAM sensing circuitry, yet such approaches require additional complexity, area overhead, speed penalty and power consumption [6], [7]. Meanwhile, as for read-disturbance-free MRAMs like SOT and VCMA, sensing margin can be enlarged by raising the readout voltage. However, the TMR ratio normally displays a negative correlation with the bias voltage [8], and it also changes under temperature and process variations [9]–[11]. Therefore, a higher read bias voltage does not necessarily guarantee a higher sensing margin, and a system capable of dynamically tracking the optimal read bias voltage to maximize the sensing margin hence becomes essential.

In this brief, we utilize a dynamic bias optimizer (DBO) to enhance MRAM readout margin. The remainder of this brief is organized as follows: Section II quantifies the theoretical optimal read bias voltage. Section III provides a detailed explanation of the schematic and operating principle of the DBO circuit. Section IV presents the simulated transient response, tracking accuracy and bit error rate improvement of the DBO-integrated 1Mb MRAM macro. Finally, Section V concludes this brief.

II. OPTIMAL BIAS VOLTAGE FOR MAXIMUM MARGIN

In general, TMR ratio of an MRAM device at a given temperature can be modeled as [12]

$$TMR(V_{REF}) = \frac{TMR(0)}{1 + \frac{V_{REF}^2}{V_h^2}} \quad (1)$$

where $TMR(0)$ represents the TMR ratio under zero bias, V_h is the characteristic voltage at which the TMR ratio drops to half of $TMR(0)$, and V_{REF} is the read bias voltage.

As illustrated in Fig. 1(b), during the MRAM read operation, both the reference and the selected bit-cell are biased at V_{REF} , which generate I_{CELL} and I_{REF} for the sense amplifier, respectively. The sensing margin (I_M) is defined as the

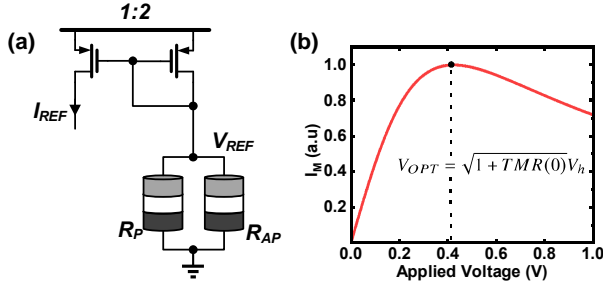


Fig. 2. (a) The schematic of an MRAM current reference. (b) Read bias voltage-dependent sensing current margin.

minimum current difference between the cell current and the reference current, that is $I_M = \min(I_P - I_{REF}, I_{REF} - I_{AP})$. I_{REF} is usually generated by the reference circuit depicted in Fig. 2(a), where the summation of I_P and I_{AP} is extracted using two parallel connected MTJ cells in the P and AP states, respectively. Afterwards, the current is scaled by a 2:1 current mirror to generate $(I_P + I_{AP})/2$ as the reference current. In this regard, the sensing margin becomes identical for both read 1 and read 0 operations, as expressed by

$$\begin{aligned} I_M &= \frac{I_P + I_{AP}}{2} - I_{AP} = I_P - \frac{I_P + I_{AP}}{2} \\ &= \frac{TMR(0)}{2R_P} \frac{1}{1 + TMR(0)} + \frac{V_{REF}}{V_h^2} \end{aligned} \quad (2)$$

Accordingly, the read bias voltage dependent I_M curve is shown in Fig. 2(b). Instead of an monotonically increasing correlation, the $I_M - V_{REF}$ curve reaches the maximum value at a certain voltage V_{OPT} , and above such an optimal point, any higher bias voltage would lead to a reduced sensing margin instead. Mathematically, V_{OPT} can be derived by taking $\frac{\partial I_M}{\partial V_{REF}} = 0$ in (2) as

$$V_{OPT} = \sqrt{1 + TMR(0)} V_h \quad (3)$$

Guided by (3), we can observe that the optimal bias point in reference to the largest sensing margin is not a constant. Instead, V_{OPT} is positively correlated with both $TMR(0)$ and V_h . As summarized in Fig. 3(a), the increase of $TMR(0)$ from 60% to 140% can result in a 30% increase in V_{OPT} . Concurrently, by appropriately adjusting the characteristic voltage V_h from 0.15 V to 0.35 V, the optimal bias point is shifted by 100% (Fig. 3(b)). It is noted that the fabrication process of the MTJ stack invariably causes discrepancies of V_h and $TMR(0)$ among different memory blocks across the die, and such variations would deteriorate as the MTJ size is scaled down. Therefore, it is important to precisely track the local optimal bias point for individual memory blocks. Moreover, both ambient thermal conditions and circuit heat dissipation would affect the operating temperature of the MRAM array, which also leads to the variations of $TMR(0)$ and V_h . For instance, Fig. 4(a) shows that both the $TMR(0)$ and V_h values decrease 30% when the MTJ bit-cell is heated from room temperature to 400 K, which in turn reduces V_{OPT} by 50% (Fig. 4(b)). Under such circumstances, real time V_{OPT} tracking is essential for high density, high speed MRAM applications.

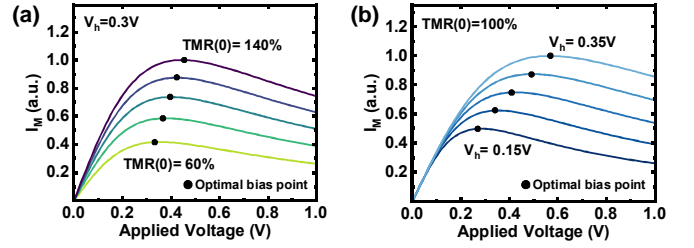


Fig. 3. Sensing margin and optimal bias voltage shift at (a) different $TMR(0)$ amplitudes under a given V_h (b) varied V_h for a fixed $TMR(0)$ value.

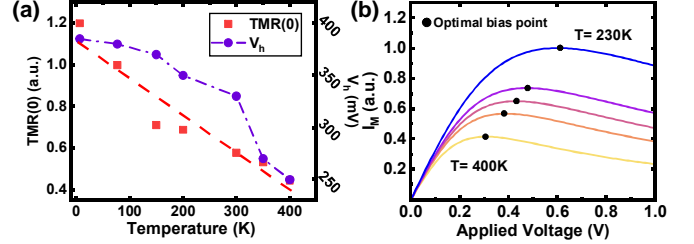


Fig. 4. (a) Temperature-dependent $TMR(0)$ and V_h of a typical MTJ bit-cell. Data extracted from [13]. (b) Read bias voltage dependent sensing margin curves at different operation temperatures.

III. DYNAMIC BIAS OPTIMIZER CIRCUIT DESIGN

The schematic of the proposed DBO circuit for MRAM read operation is illustrated in Fig. 5. In general, the DBO generates reference voltage V_{REF} to approximate V_{OPT} with a feedback system, which consists of three main blocks: 1. a margin extraction circuit that extracts sensing margin I_M and converts it to voltage margin V_M , 2. a control logic block that periodically samples V_M to determine the tuning direction of V_{REF} , and 3. a charge pump module that feeds back the updated V_{REF} value to the margin extraction circuit as reference voltage in the next cycle.

Specifically, the margin extraction circuit is composed of two active clamp circuits, current mirrors, a trans-impedance amplifier (TIA), and a source follower. To accurately replicate the cell current, MC1/A1 and MC2/A2 regulate the voltage on the reference MTJs to V_{REF} , ensuring the current on each path is $I_P = V_{REF}/R_P$ and $I_{AP} = V_{REF}/R_{AP}$, respectively. Meanwhile, the current mirror M1/M2 subtracts I_{AP} from I_P to obtain the sensing current margin I_M . Subsequently, I_M is converted to V_M through TIA $M3/M4/R_{REF}$, following $V_M = R_{REF} \times W4/W3 \times I_M$. Finally, a source follower isolates the TIA from the control circuits, which not only protects the margin extraction circuit from kickback, but also provides higher driving strength.

Next, in view of the control logic block, it comprises a sample/hold circuit, a comparator, a toggle flip-flop, a latch, and combinational logic. The output voltage V_M from the margin extraction circuit is periodically sampled and stored as V_S . The comparator compares V_S and V_M to detect the change of V_M , and the FLIP signal determines whether the tuning direction of V_{REF} needs to be adjusted. Additionally, a COARSE flag, set by the FLIP signal, configures the incremental step of V_{REF} . In this regard, based on the FLIP and COARSE signals, the control logic generates UP_C, UP_F, and DN signals for the charge pump module.

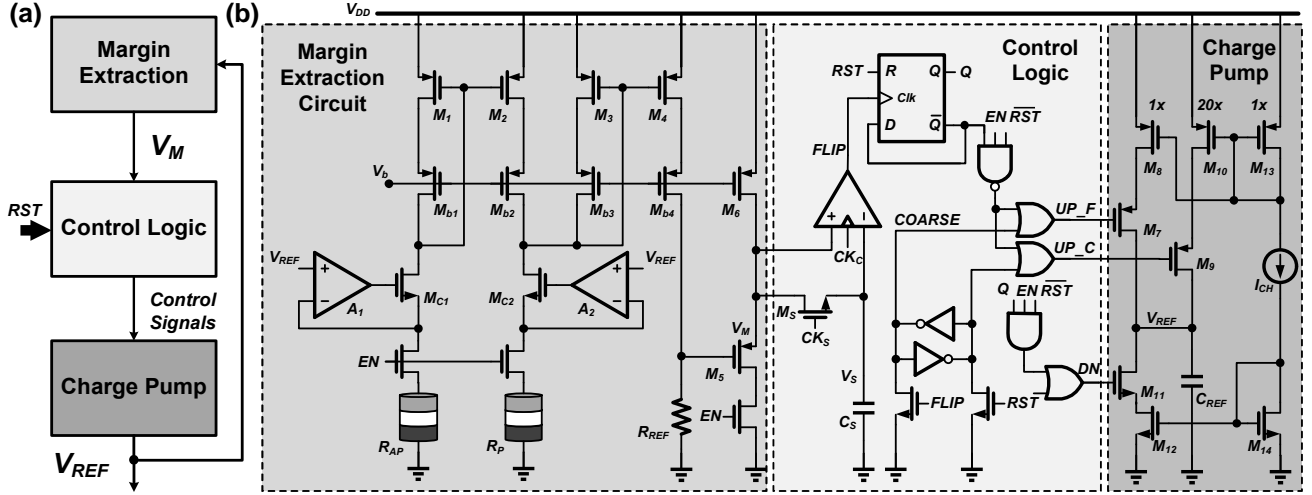


Fig. 5. (a) Block diagram of the proposed DBO with feedback mechanism which dynamically tracks sensing margin and generate V_{REF} for MRAM read operations. (b) Detailed schematic of the DBO circuit, which includes margin extraction circuit, control logic block and the charge pump module.

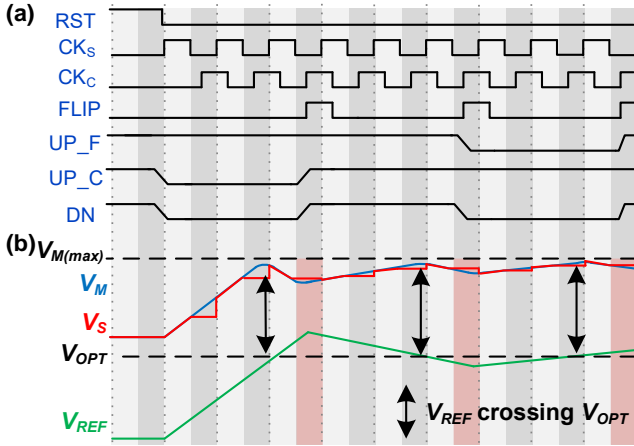


Fig. 6. Operation waveforms of the DBO circuit, from initialization to the steady state, with V_{REF} crossing V_{OPT} (marked with arrow) and FLIP events (highlighted with red background).

Finally, a charge pump module updates V_{REF} according to the output signals from the control logic block. In this stage, a bias circuit M13/M14 determines the minimum update step in V_{REF} . The current source M7/M8, enabled by UP_F, provides a fine-tuned increase in V_{REF} , while M9/M10, enabled by UP_C, provides a coarse increase of V_{REF} with $20\times$ step because of the transistor width ratio between M10 and M8. Conversely, M11/M12, enabled by DN, pulls down the V_{REF} with $1\times$ step. Therefore, the combination of the coarse-fine paths significantly reduces the settling time during power up and exit from sleep.

Accompanying with the DBO circuit implementation, the corresponding operation waveforms and real-time sensing margin tracking mechanism are visualized in Fig. 6. Initially, V_{REF} and all latches/flip-flops are reset to 0. Once the DBO is activated, M7/M11 are turned off, while M9 is switched on to enable a fast slewing in V_{REF} . In the meantime, the sample/hold circuit samples V_M to V_S at every falling edge of CK_S . At the end of each hold phase, the comparator that is triggered by CK_C would determine the output FLIP

state. In particular, as long as V_{REF} approaches V_{OPT} , the sensing margin increases (i.e., $V_M > V_S$), and the FLIP signal remains 0 (i.e., indicative of the same charging direction). On the other hand, when the read bias V_{REF} crosses away from the optimal bias point, as illustrated in Fig. 2(b). As a result, once the current V_M becomes lower than V_S , the FLIP signal is triggered to toggle the charging direction of the charge pump module for the next sampling cycle, and the circuit converges to the optimal $V_{REF} = V_{OPT}$ with a periodic toggling of the FLIP signal in the steady state, therefore realizing the real-time tracking of V_{REF} in reference to the V_{OPT} baseline, as shown in Fig. 6(b). It is noted that the first FLIP signal after initialization sets the COARSE flag to 0, hence automatically driving the charge pump stage into the fine-tuning phase to provide a more refined tracking of V_{OPT} .

IV. 1MB MRAM SIMULATION

Following the aforementioned read margin optimization method, an 1Mb MRAM macro with the real-time dynamic bias adjustment function was designed, as depicted in Fig. 7. The macro is organized with 64 blocks, each of which consists a 512×34 array with 32 data bit-lines (BL) and 2 reference BLs. Row and column drivers are placed adjacent to the MRAM bit-cell array, which generate WL and YSEL signals for bit-cell selection. To track block level V_{OPT} variation, a DBO module is embedded in each block next to the sense amplifier (SA). It is also seen from Fig. 7 that the DBOs share cells with the reference columns in the block so as to save layout area. During initialization or exit from sleep, the DBOs help stabilize V_{REF} towards V_{OPT} . After stabilization, the DBOs periodically monitor the evolution of V_{OPT} due to temperature induced $TMR(0)$ and V_h drifts, and make dynamic adjustment to V_{REF} accordingly. Besides, each DBO unit is activated individually with $1/64$ duty cycle in steady state to reduce power overhead. The performance of the DBO-embedded 1Mb MRAM was evaluated using a 28-nm CMOS process design kit (PDK), and a physical MTJ device model

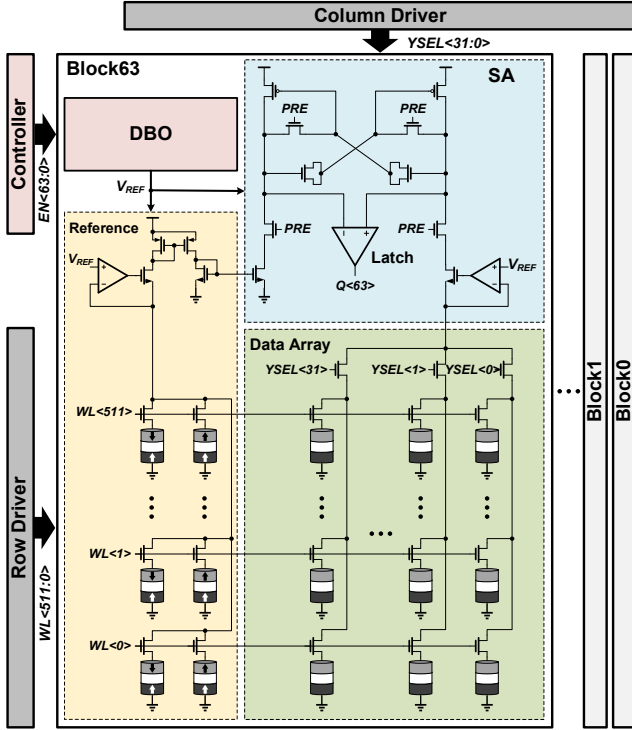


Fig. 7. High-level architecture of DBO-enhanced MRAM readout path.

TABLE I
KEY PARAMETERS ADOPTED FOR SIMULATION

Parameter	Description	Value
α	LLGE damping factor	0.02
M_S	Saturation magnetization	1.2×10^6 A/m
K_i	Anisotropy field constant	1.0×10^{-3} J/m ²
X_i	VCMA field constant	80×10^{-15} J/(V·m)
t_{ox}	Oxide barrier height	1.4nm
t_{fl}	Free layer thickness	1.1nm
W, L	MTJ width and length	60nm
R_p	Parallel resistance	10k Ω
$TMR(0)$	@RT TMR ratio with 0 bias	100%
	@125°C	70%
V_h	@RT Half TMR voltage	0.3V
	@125°C	0.22V

in Verilog-A was used to capture the key parameters from reported measurement results (Table I) [14]. In addition, we also included the temperature-dependent $TMR(0)$ and V_h data adopted from [13] to warrant the reliability of high-temperature simulations.

Fig. 8 presents the post-layout simulation results of the designed DBO circuit at room temperature. During the simulation, the sampling rate is set at 5 MHz, and the coarse and fine voltage steps are 80 mV and 4 mV per cycle, respectively. It can be clearly observed from Fig. 8(c) that the V_{REF} curve slews swiftly under the coarse tuning mode during initialization. Afterwards, the control logics promptly responds with FLIP signal pulses whenever V_{REF} crosses V_{OPT} . Eventually, the system successfully converges to $(100\% \pm 2\%)V_{OPT}$ within 2 μ s, or 10 cycles, with a ± 10 mV ripple in steady state.

Apart from the V_{OPT} real-time tracking function validation, the DBO tracking capability under different MTJ electrical parameters and thermal conditions are also evaluated. As illustrated in Fig. 9(a), within the examined range where $TMR(0)$ and V_h vary from 60% to 120% and from 0.2 V to 0.35 V

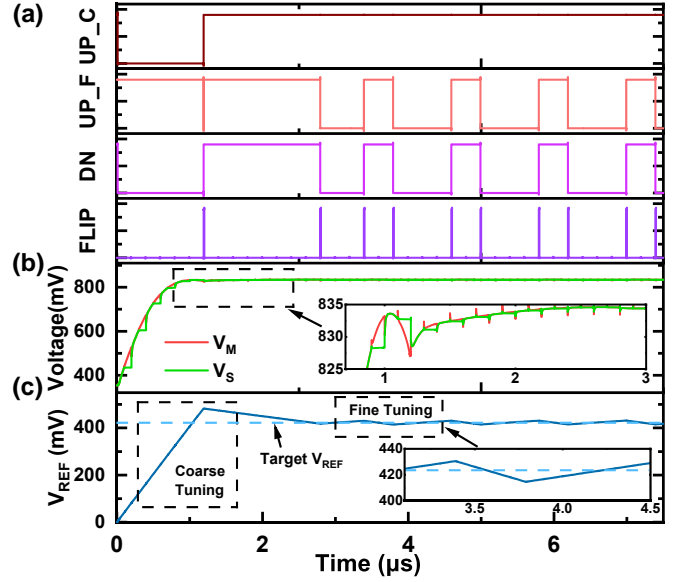


Fig. 8. Simulation waveforms of proposed DBO, showing (a) critical control signals (b) V_M , V_S and (c) output V_{REF} .

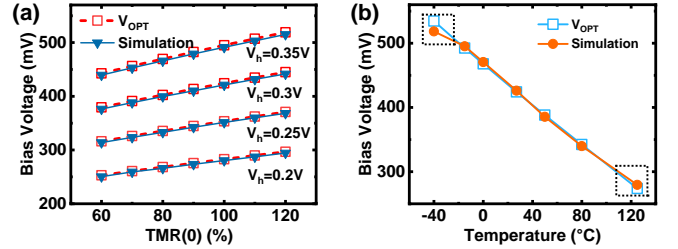


Fig. 9. DBO tracking accuracy under different (a) $TMR(0)$ and V_h of MTJ, and (b) thermal conditions.

respectively, the DBO-adjusted bias voltage V_{REF} manages to follow the evolution of V_{OPT} with the tracking accuracy above 98%, hence justifying a wide functional range. Likewise, our DBO also exhibits a highly-consistent performance over a wide temperature range from -40 °C to 125 °C, and the V_{REF} value only slightly deviates from the ideal V_{OPT} baseline at extreme high and low temperatures, possibly due to the headroom compression of the current mirrors (M1-M4) and a reduced sensitivity of the comparator in the control logic stage, as shown in Fig. 9(b). Furthermore, by introducing the temperature variation of $TMR(0)$ and V_h during simulation, the transient V_{REF} waveform is able to respond to the rapid temperature drift rate of 98 °C/ms (Fig. 10(a)), and the readout sensing margin improves by 20% compared to that of the MRAM block without DBO, as highlighted in Fig.10(b). Consequently, the above results evince the advantage of DBO in optimizing the read performance of the MRAM array against process and thermal variations.

Finally, Fig. 11 examines the bit error rate of the 1Mb MRAM macro with (blue circles) and without (red squares) the DBO module by taking into account different degrees of variation-to-mean ratios (σ/μ) in V_h and $TMR(0)$. Strikingly, the simulation results at both temperatures consistently confirm that the DBO helps to reduce the bit error rate by 1 to 2 orders of magnitude. From Table II, it can be referred that under the same physical parameters, MRAM array with DBO

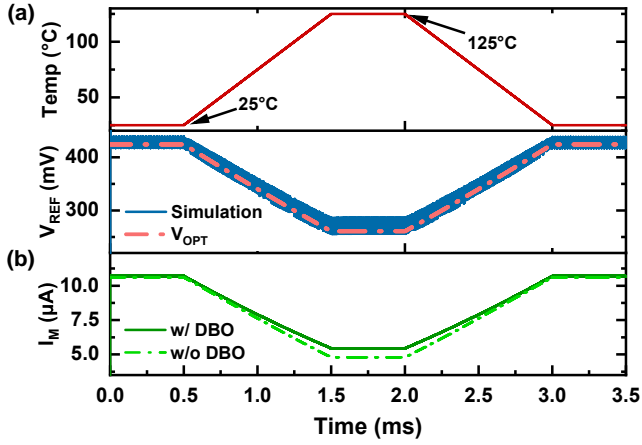


Fig. 10. (a) Simulated DBO regulated V_{REF} transient response to rapid temperature change and (b) corresponding sensing margins with (solid line) and without (dashed line) DBO.

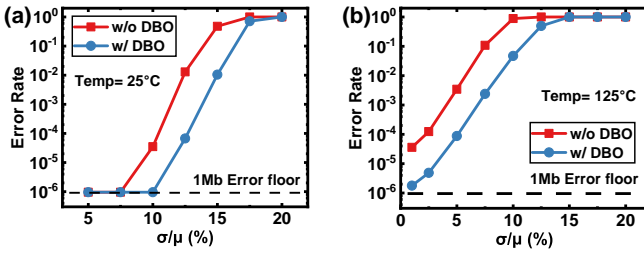


Fig. 11. Simulated bit error rate of 1Mb MRAM macro with (blue circles) and without (red squares) DBO versus process variation at (a) $T = 25^\circ\text{C}$, and (b) $T = 125^\circ\text{C}$.

TABLE II
1MB MRAM PERFORMANCE COMPARISON

	w/DBO	w/o DBO. optimized for 25°C	w/o DBO. optimized for 125°C
Technology	28-nm		
Macro size	1Mb		
TMR(0)@ 25°C [%]	100		
Assumed σ/μ [%]	5		
Operation BER*	8.71×10^{-5}	3.45×10^{-3}	1.27×10^{-3}
Read Power [mW]	4.07	3.94	3.91
Layout Area [mm^2]	0.242	0.229	0.229

* Operation bit error rate (BER) is the maximum BER under temperature range from 25°C to 125°C

provides more than $10\times$ improvement in bit readout accuracy over fixed reference voltages, which is at the expense of a 5% power overhead and a 6% extra layout area penalty.

V. SUMMARY

In conclusion, the optimal bias condition for the MRAM readout operation is quantitatively investigated and a DBO-modulated V_{REF} is proposed to warrant the largest sensing margin as well as to effectively accommodate the V_{OPT} variation within the MRAM array. The 1Mb MRAM simulation results demonstrate a $>98\%$ tracking accuracy regardless of PVT variations. Furthermore, through Monte Carlo simulations, the DBO also brings about $10\times$ to $100\times$ improvements in readout yield. Based on the generic feedback principle and margin extraction mechanism, advanced searching algorithm can be applied to the DBO circuit to further improve the V_{OPT} tracking efficiency for high-density MRAM applications.

REFERENCES

- [1] S. Ikegawa, F. B. Mancoff, J. Janesky, and S. Aggarwal, "Magnetoresistive random access memory: Present and future," *IEEE Trans. Electron Devices*, vol. 67, no. 4, pp. 1407–1419, Apr. 2020.
- [2] Q. Dong, Z. Wang, J. Lim *et al.*, "A 1Mb 28nm STT-MRAM with 2.8ns read access time at 1.2V VDD using single-cap offset-cancelled sense amplifier and in-situ self-write-termination," in *IEEE Int. Solid-State Circuits Conf. (ISSCC)*, 2018, pp. 480–482.
- [3] K. C. Chun, H. Zhao, J. D. Harms, T.-H. Kim, J.-P. Wang, and C. H. Kim, "A scaling roadmap and performance evaluation of in-plane and perpendicular MTJ based STT-MRAMs for high-density cache memory," *IEEE J. Solid-State Circuits*, vol. 48, no. 2, pp. 598–610, Feb. 2013.
- [4] Q. Shao, P. Li, L. Liu *et al.*, "Roadmap of spin-orbit torques," *IEEE Trans. Magn.*, vol. 57, no. 7, pp. 1–39, Jul. 2021.
- [5] P. Khalili Amiri, J. G. Alzate, X. Q. Cai *et al.*, "Electric-field-controlled magnetoelectric RAM: Progress, challenges, and scaling," *IEEE Trans. Magn.*, vol. 51, no. 11, pp. 1–7, Nov. 2015.
- [6] Y. Zhou, H. Cai, B. Liu, W. Zhao, and J. Yang, "MTJ-LRB: Proposal of MTJ-based loop replica bitline as MRAM device-circuit interaction for PVT-robust sensing," *IEEE Trans. Circuits Syst. II*, vol. 67, no. 12, pp. 3352–3356, Dec. 2020.
- [7] T. Na, J. Kim, B. Song, J. P. Kim, S. H. Kang, and S.-O. Jung, "An offset-tolerant dual-reference-voltage sensing scheme for deep submicrometer STT-RAM," *IEEE Trans. VLSI Syst.*, vol. 24, no. 4, pp. 1361–1370, Apr. 2016.
- [8] S. Yuasa, T. Nagahama, A. Fukushima, Y. Suzuki, and K. Ando, "Giant room-temperature magnetoresistance in single-crystal Fe/MgO/Fe magnetic tunnel junctions," *Nature materials*, vol. 3, pp. 868–71, 2004.
- [9] B. Jinnai, J. Igarashi, K. Watanabe *et al.*, "High-performance shape-anisotropy magnetic tunnel junctions down to 2.3 nm," in *IEEE Int. Electron Devices Meeting (IEDM)*, 2020, pp. 24.6.1–24.6.4.
- [10] C.-T. Chao, C.-C. Chen, C.-Y. Kuo *et al.*, "Temperature dependence of electrical transport and magnetization reversal in magnetic tunnel junction," *IEEE Trans. Magn.*, vol. 46, no. 6, pp. 2195–2197, Jun. 2010.
- [11] Y. J. Song, J. H. Lee, S. H. Han *et al.*, "Demonstration of highly manufacturable STT-MRAM embedded in 28nm logic," in *IEEE Int. Electron Devices Meeting (IEDM)*, 2018, pp. 18.2.1–18.2.4.
- [12] Y. Zhang, W. Zhao, Y. Lakys *et al.*, "Compact modeling of perpendicular-anisotropy CoFeB/MgO magnetic tunnel junctions," *IEEE Trans. Electron Devices*, vol. 59, no. 3, pp. 819–826, Mar. 2012.
- [13] M.-C. Hong, Y.-J. Chang, Y.-C. Hsin *et al.*, "A 4K–400K wide operating-temperature-range MRAM technology with ultrathin composite free layer and magnesium spacer," in *Proc. IEEE Symp. VLSI Technol. Circuits*, 2022, pp. 379–380.
- [14] S. Wang, H. Lee, F. Ebrahimi, P. K. Amiri, K. L. Wang, and P. Gupta, "Comparative evaluation of spin-transfer-torque and magnetoelectric random access memory," *IEEE Trans. Emerg. Sel. Topics Circuits Syst.*, vol. 6, no. 2, pp. 134–145, Jun. 2016.